Simulation Modelling Practice and Theory 134 (2024) 102953

Contents lists available at ScienceDirect

Simulation Modelling Practice and Theory

journal homepage: www.elsevier.com/locate/simpat

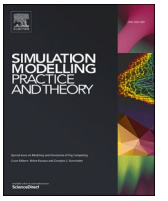

Modelling and dynamic characterisation of a double-pendulum overhead crane carrying a distributed-mass payload

M.M. Bello [a,b], Z. Mohamed [a,*], M.Ö. Efe [c], H. Ishak [a]

[a] Faculty of Electrical Engineering, Universiti Teknologi Malaysia, 81310 Johor Bahru, Johor, Malaysia
[b] Mechatronics Engineering Department, Faculty of Engineering, Bayero University, Kano, Nigeria
[c] Department of Computer Engineering, Hacettepe University, Turkey

ARTICLE INFO

Keywords:
Double-pendulum crane
Distributed-mass payload
Dynamic characteristics
Modelling
Payload hoisting

ABSTRACT

In industries, cranes are commonly used for transportation of a distributed-mass payload (DMP). However, analysis of the dynamic characteristics of such a system is limited since most of the research work considered a point-mass payload. This paper presents modelling and analysis of dynamic characteristics of a double-pendulum overhead crane carrying a DMP with and without payload hoisting. Nonlinear dynamic models representing the crane in both scenarios are derived. The effects of varying cable lengths, and carrying different payload masses and lengths on the dynamics of hook and payload oscillations are also studied. Simulations are performed to observe the dynamic characteristics of the crane under several conditions, and experiments are carried out to validate the theory and simulation results, and to assess the accuracy of the derived nonlinear dynamic equations. The results demonstrate that the payload oscillation is significantly affected by changes in the cable lengths and DMP parameters. In addition, satisfactory agreements between simulation and experimental results are achieved, which indicate validity of the nonlinear models and good compliance with the theory. It is envisaged that the dynamic characteristic analyses of the crane can be beneficial in designing efficient controllers, especially in suppressing DMP oscillation.

1. Introduction

A crane system is a machine that assists with lifting, moving, and transporting heavy objects. It is utilized in many industries, such as construction, manufacturing, transportation, and logistics. The main parts of a crane system are the hoist, which moves objects vertically, and the trolley or carriage, which moves objects horizontally on a rail or beam. Cranes can be mounted on structures such as gantries, towers, or overhead beams to increase stability and range of motion [1]. Different types of crane systems are used for various tasks and environments because of their unique advantages and limitations. They play a crucial role in enhancing productivity and efficiency in industries that handle large objects. Moreover, labour-intensive activities become safer and more efficient with the use of crane systems in a wide range of industrial contexts [2]. Cranes can be classified as single mode or multi-mode types depending on the link and drive mechanism in them. A specialised crane system, known as a "double crane", is characterised by its double pendulum-like mechanism, which distinguishes it from conventional single-pendulum cranes. This design offers enhanced movement and flexibility by utilising two interconnected pendulums with independent motion. As a result, it creates a more intricate lifting and moving system

* Corresponding author.
E-mail address: zahar@fke.utm.my (Z. Mohamed).

https://doi.org/10.1016/j.simpat.2024.102953
Received 22 November 2023; Received in revised form 27 March 2024; Accepted 2 May 2024
Available online 3 May 2024

within the context of crane operations [3]. However, due to their complex design and increased mobility, specialised training and advanced control systems may be necessary to ensure safe and efficient operations.

In addition, cranes are utilised for the conveyance of two distinct types of loads, namely point-mass payload (PMP) and distributed-mass payload (DMP), which are differentiated based on their mass distribution. A PMP is utilised in engineering studies to simplify calculations when the load's weight is concentrated in a single location, which is frequently the case when the load's dimensions are smaller than the crane's capabilities [4]. Although most payloads have weight distributions that are not fully concentrated at a single point, applying a point mass approximation can be a valid approach when considering a crane's strength and stability. Besides, DMPs account for the payload's actual weight distribution as the weight being lifted is not always evenly distributed over its length, width, or height [5]. For example, a lengthy beam or a container, may have varied weight distributions over its length. When dealing with a DMP, the crane's capability and structural concerns must take the fluctuating weight distribution into account. This includes elements such as the payload's centre of gravity and various forces placed on the crane's components throughout lifting, moving, and placing operations [6]. In essence, the key difference between PMP and DMP in a crane system is how the payload's weight is addressed. The weight of the payload is concentrated at a single point in PMP, which simplifies computations, but may not correctly reflect real-world situations. In contrast, DMP accounts for the actual weight distribution of the payload, giving a more accurate description of its effect on the functionality and structural integrity of the crane.

In the literature, although a significant work has been reported on the dynamics and control of a double-pendulum crane, a majority of the works focus on the PMP. Recently, researchers have turned their attention to DMP, and a limited number of articles have been published which mainly investigated efficient control approaches for various cranes. The controllers can be categorised into feed-forward and feedback control approaches. The feedforward control includes command smoothing for a bridge crane [7,8], a new input shaping for a tower crane [9,10], a trajectory planning method for a bridge crane [11] and an optimal smoother for an overhead crane [12]. In the most recent work, a command smoother for a tower crane [13] was proposed. In designing feedforward controllers, the crane dynamic parameters including frequencies and damping ratios of oscillations are usually required to suppress the hook and DMP sways. Besides, the feedback control techniques include time-varying Sliding Mode Control (SMC) for a bridge crane [14], an equivalent rope length trajectory planning [15], a combination of quasi-periodicity theory with a trajectory planning controller [16] and an adaptive control to achieve positioning and swing elimination of a three-dimensional overhead crane [17]. Most recently, deep reinforcement learning-based control was proposed for a triple pendulum crane system [18].

As only a few studies that focus on DMP have been conducted, the efforts towards modelling and control of DMP have remarkable merits for industrial crane experts. In designing high performance controllers, both in feedforward and feedback control approaches, good understanding on the dynamic characteristics of a double-pendulum crane carrying DMP is important. In practice, cranes are also subjected to carrying DMPs with different masses and lengths during their operations. In this case, understanding of their effects on the crane's dynamics, especially in terms of the hook and DMP oscillations, will be very helpful. Another essential crane operation is payload hoisting, in which a DMP is carried from one height to another for a pick and place operation. This results in varying cable lengths, which also affects the dynamics of the oscillations. However, comprehensive knowledge on these issues is limited as none of the previous works investigated the effects of mass and length of DMP on the crane dynamics, especially with both simulation and experimental works. Furthermore, none of the works reported previously studied modelling and dynamic characterisation during simultaneous trolley motion and payload hoisting of DMP.

This paper presents dynamic characterisations of a double-pendulum overhead crane (DPOC) carrying DMP without and with payload hoisting. Dynamic models of the crane under both scenarios are derived by using the Lagrange equation, and experiments are conducted on a laboratory DPOC. The crane's dynamic characteristics especially in terms of the hook and DMP oscillations are observed. This work also evaluates the effects of varying cable lengths during payload hoisting, and carrying different DMP masses and lengths on the system dynamics. The validity and accuracy of the nonlinear equations describing the dynamics are evaluated by comparing the simulation and experimental results under various testing conditions. With respect to the existing body of literature, this paper contributes in the following aspects:

a) Dynamic models of a DPOC with DMP without and with payload hoisting have been derived. To the best of our knowledge, this is the first study on a DMP with payload hoisting. The derived models have been validated via a set of experiments.
b) This paper provides a comprehensive analysis of the dynamic characteristics of a DPOC carrying DMP, focuses on the hook and DMP oscillations. These are useful in designing effective controllers especially in the feedforward control approach.
c) This paper evaluates the effects of payload hoisting (varying cable lengths) and carrying different DMP masses and lengths on the crane's dynamics. Such a work is limited in the literature. This knowledge is also important in controller designs as these are practical scenarios in crane operations.

2. Dynamic modelling

The method of Lagrangian is the preeminent and extensively employed approach for the purpose of modelling a system of double-pendulum crane [19]. The approach that involves identifying the Lagrange equation is well-suited for this type of system. To illustrate the differences between the two models, initially a DPOC with PMP is briefly described. Then, concise representations for the modelling of the DPOC carrying a DMP without and with the hoisting cable length are presented.

2.1. A DPOC with PMP

Fig. 1 shows a schematic diagram of a DPOC system with a point-mass payload. The crane system is composed of three generalised independent coordinates, namely, the trolley position, x, the hook angle, θ, and the payload angle φ. The parameters $m_t, m_h, m_p, l_1, l_2, f_x$ and g represent the trolley mass, hook mass, payload mass, massless cable length between trolley and hook, massless cable length between hook and payload, trolley viscous damping coefficients and the gravitational constant respectively. Additionally, F_x denotes an externally applied force to the crane, which is the sole input for the system. Fig. 1(a) shows a case of a constant cable length, whereas Fig. 1(b) illustrates a case of payload hoisting. In Fig. 1(b), F_l is the force required to lift the payload and f_l illustrates the viscous damping coefficients.

Using this assumption, the payload is considered as a lump mass with all its weight concentrated at one point. This simplification makes calculations and simulations much faster and easier, letting researchers to focus on the main forces and movements involved. The Lagrangian method was used to obtain the dynamic equations of the crane systems [19].

For a fixed cable length, the Lagrangian function based on the kinetic and potential energies can be obtained as:

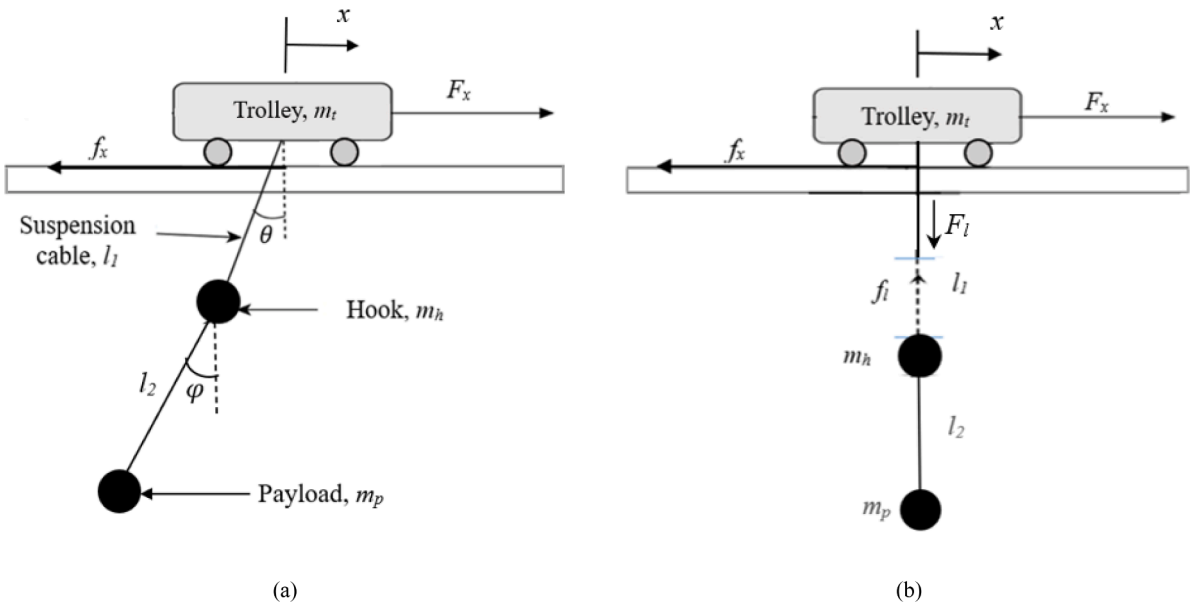

Fig. 1. DPOC with a point-mass payload, (a) Fixed length, (b) Hoisting.

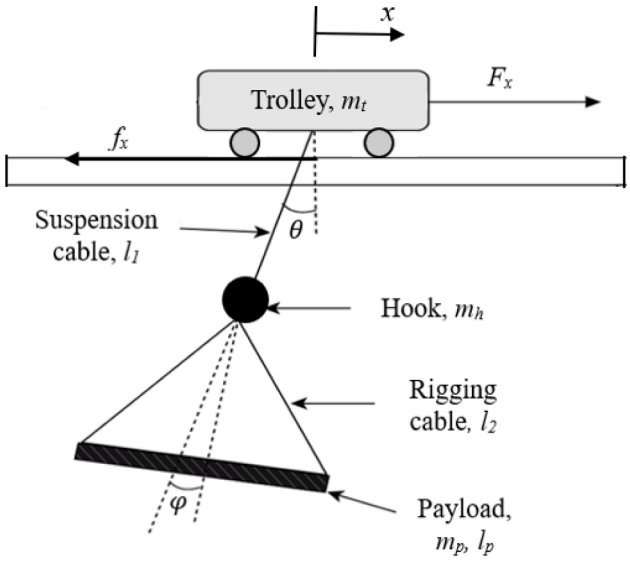

Fig. 2. Double-pendulum overhead crane with DMP.

$$L = \frac{1}{2}\left(m_t + m_h + m_p\right)\dot{x}^2 + \left(m_h + m_p\right)\dot{x}l_1\dot{\theta}\cos\theta + \frac{1}{2}\left(m_h + m_p\right)l_1{}^2\dot{\theta}^2 + \frac{1}{2}m_p\left[l_2{}^2\dot{\varphi}^2 + 2\dot{x}l_2\dot{\varphi}\cos\varphi + 2l_1l_2\dot{\theta}\dot{\varphi}\cos(\theta-\varphi)\right] - \left(m_h + m_p\right)gl_1(1-\cos\theta) - m_pgl_2(1-\cos\varphi) \tag{1}$$

On the other hand, for the case with payload hoisting, l_1 is varying during the crane motion and thus becomes another independent coordinate. The Lagrangian function can be written as:

$$L_{hoist} = \frac{1}{2}\left(m_t + m_h + m_p\right)\dot{x}^2 + \frac{1}{2}\left(m_h + m_p\right)\left[2\dot{x}\dot{l}_1\dot{\theta}\cos\theta + 2\dot{x}\dot{l}_1\sin\theta + l_1{}^2\dot{\theta}^2 + \dot{l}_1{}^2\right] + \frac{1}{2}m_p\left[2\dot{x}l_2\dot{\varphi}\cos\varphi + 2l_1l_2\dot{\theta}\dot{\varphi}\cos(\theta-\varphi) + 2\dot{l}_1l_2\dot{\varphi}\sin(\theta-\varphi) + l_2{}^2\dot{\varphi}^2\right] - \left(m_h + m_p\right)gl_1(1-\cos\theta) - m_pgl_2(1-\cos\varphi) \tag{2}$$

2.2. A DPOC with DMP

Fig. 2 illustrates a schematic diagram of a DPOC system that carries a DMP with a cable length remain constant. The main differences as compared to the PMP model in Fig. 1 are:

- A distributed-mass payload is considered with payload length, l_p.
- Two massless rigging cables with length, l_2 are introduced to hold the horizontal payload.
- The payload angle, φ is measured with respect to the centre point of the distributed payload.

Similarly, the Lagrange method can be utilised to examine the dynamic model of the crane with a constant cable length [14,20]. The Lagrangian equation in terms of the generalised coordinate, q_i can be written as:

$$\frac{d}{dt}\left(\frac{\partial L}{\partial \dot{q}_i}\right) - \frac{\partial L}{\partial q_i} = T \tag{3}$$

where,

$$L = E_K - E_P \tag{4}$$

L, E_K and E_P are the Lagrangian, kinetic and potential energies respectively. q_i represents x, θ and φ.

2.2.1. A fixed length

Based on the schematic diagram in Fig. 2, the kinetic energy of the system can be obtained as:

$$E_K = \frac{1}{2}m_t\dot{x}^2 + \frac{1}{2}m_h(\dot{x} - l_1\dot{\theta}\cos\theta)^2 + \frac{1}{2}m_h(\dot{x} - l_1\dot{\theta}\sin\theta)^2 + \frac{1}{2}m_p(\dot{x} - l_1\dot{\theta}\cos\theta - l_2\dot{\varphi}\cos\varphi)^2 + \frac{1}{2}m_p(l_1\dot{\theta}\sin\theta - l_2\dot{\varphi}\sin\varphi)^2 + \frac{1}{2}J\dot{\varphi}^2 \tag{5}$$

where the last term, $\frac{1}{2}J\dot{\varphi}^2$ is called autobiographical perturbation of kinetic energy of the payload, and J is the moment of inertia of the payload given as:

$$J = \frac{1}{12}m_pl_p{}^2 \tag{6}$$

The potential energy can be obtained as:

$$E_P = m_hgl_1(1-\cos\theta) + m_pg(l_1 - l_1\cos\theta + l_2 - l_2\cos\varphi) \tag{7}$$

Since payload twisting motion is not considered in this work, the potential energy in Eq. (7) is not affected by the payload length, l_p. Therefore, the Lagrangian function using the system's kinetic and potential energies can be written as:

$$L = \frac{1}{2}\left(m_t + m_h + m_p\right)\dot{x}^2 - \left(m_h + m_p\right)l_1\dot{x}\dot{\theta}\cos\theta - \frac{1}{2}\left(m_h - m_p\right)l_1{}^2\dot{\theta}^2 - m_pl_2\dot{x}\dot{\varphi}\cos\varphi + m_pl_1l_2\dot{\theta}\dot{\varphi}\cos(\theta-\varphi) + \frac{1}{2}m_p\left(l_2{}^2 + \frac{1}{12}l_p{}^2\right)\dot{\varphi}^2 - \left(m_h + m_p\right)gl_1 + \left(m_h + m_p\right)gl_1\cos\theta - m_pgl_2 + m_pgl_2\cos\varphi \tag{8}$$

The function in Eq. (8) can be shown to be different when compared to its counterpart in Eq. (1). The nonlinear dynamic model of the crane system can finally be obtained by differentiating Eq. (8) and obtaining terms as in Eq. (3) as:

$$\left(m_t + m_h + m_p\right)\ddot{x} - \left(m_h + m_p\right)l_1\ddot{\theta}\cos\theta + \left(m_h + m_p\right)l_1\dot{\theta}^2\sin\theta - m_pl_2\ddot{\varphi}\cos\varphi + m_pl_2\dot{\varphi}^2\sin\varphi = F - f_x\dot{x} \tag{9}$$

$$-\left(m_h + m_p\right)l_1\ddot{x}\cos\theta - \left(m_h - m_p\right)l_1{}^2\ddot{\theta} + m_pl_1l_2\ddot{\varphi}\cos(\theta-\varphi) + m_pl_1l_2\dot{\varphi}^2\sin(\theta-\varphi) + \left(m_h + m_p\right)gl_1\sin\theta = 0 \tag{10}$$

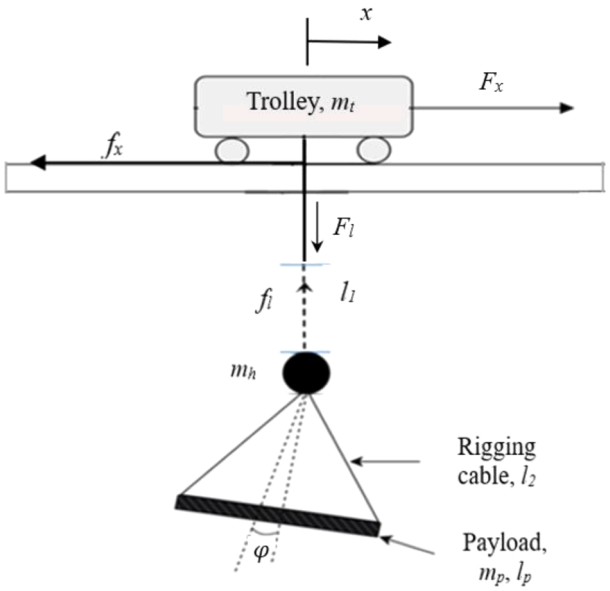

Fig. 3. A schematic diagram of a DPOC with DMP hoisting.

$$-m_p l_2 \ddot{x}\cos\varphi + m_p l_1 l_2 \ddot{\theta}\cos(\theta-\varphi) + m_p\left(l_2{}^2 + \frac{1}{12}l_p{}^2\right)\ddot{\varphi} - m_p l_1 l_2 \dot{\theta}^2 \sin(\theta-\varphi) + m_p g l_2 \sin\varphi = 0 \tag{11}$$

2.2.2. With payload hoisting (Varying cable length)

During the process of hoisting, it is common for the length l_1 of the cable to fluctuate. This occurs as the payload is lifted up and down in order to reach a desired destination [21]. When considering the hoisting, it is necessary to take into account an extra independent generalised coordinate, q_4 in order to properly represent l_1 in the Lagrangian equation. A schematic diagram of a DPOC with DMP hoisting is shown in Fig. 3.

It is found that varying l_1 affects the kinetic energy equation, but the potential energy given in Eq. (7) is not affected. The new kinetic energy can be written as:

$$\begin{aligned} E_K &= \frac{1}{2}m_t \dot{x}^2 + \frac{1}{2}m_h(\dot{x} - l_1\ddot{\theta}\cos\theta - \dot{l}_1\sin\theta)^2 + \frac{1}{2}m_h(l_1\ddot{\theta}\sin\theta - \dot{l}_1\cos\theta)^2 + \frac{1}{2}J\dot{\varphi}^2 \\ &+\frac{1}{2}m_p(\dot{x} - l_1\ddot{\theta}\cos\theta - l_2\ddot{\varphi}\cos\varphi - \dot{l}_1\sin\theta)^2 + \frac{1}{2}m_p(l_1\ddot{\theta}\sin\theta + l_2\ddot{\varphi}\sin\varphi - \dot{l}_1\cos\theta)^2 \end{aligned} \tag{12}$$

Hence,

$$\begin{aligned} E_K &= \frac{1}{2}(m_t + m_h + m_p)\dot{x}^2 - (m_h + m_p)(\dot{x}l_1\ddot{\theta}\cos\theta + \dot{x}\dot{l}_1\sin\theta) + \frac{1}{2}(m_h + m_p)* \\ &(l_1{}^2\ddot{\theta}^2 + \dot{l}_1{}^2) - m_p\left(\dot{x}l_2\ddot{\varphi}\cos\varphi - l_1 l_2\ddot{\theta}\ddot{\varphi}\cos(\theta-\varphi) - l_2\dot{l}_1\dot{\varphi}\sin(\theta-\varphi) - \frac{1}{24}l_p{}^2\dot{\varphi}^2 - l_2{}^2\dot{\varphi}^2\right) \end{aligned} \tag{13}$$

Therefore, the new Lagrangian function can be expressed from Eqs. (7) and (13) as:

$$\begin{aligned} L_{hoist} &= \frac{1}{2}(m_t + m_h + m_p)\dot{x}^2 + \frac{1}{2}(m_h + m_p)\left(-2\dot{x}l_1\ddot{\theta}\cos\theta - 2\dot{x}\dot{l}_1\sin\theta + l_1{}^2\dot{\theta}^2 + \dot{l}_1{}^2\right) \\ &+\frac{1}{2}m_p\left(-2\dot{x}l_2\ddot{\varphi}\cos\varphi + l_2{}^2\dot{\varphi}^2 - 2l_2\dot{l}_1\dot{\varphi}\sin(\theta-\varphi) - 2l_1 l_2\dot{\theta}\ddot{\varphi}\cos(\theta-\varphi) + \frac{1}{12}l_p{}^2\dot{\varphi}^2\right) \\ &-(m_h + m_p)gl_1(1-\cos\theta) + m_p g l_2(1-\cos\varphi) \end{aligned} \tag{14}$$

The function in Eq. (14) is more complicated with more non-linear terms as compared to the case with the PMP model in Eq. (2). Solving Eq. (14) yields Eqs. (15)–(18) that represent a dynamic model of a DPOC system with DMP under hoisting operation.

$$(m_t + m_h + m_p)\ddot{x} - (m_h + m_p)\left(2\dot{l}_1\dot{\theta}\cos\theta + l_1\ddot{\theta}\cos\theta - l_1\dot{\theta}^2\sin\theta + \ddot{l}_1\sin\theta\right) - m_p l_2(\ddot{\varphi}\cos\varphi - \dot{\varphi}^2\sin\varphi) = F_x - f\dot{x} \tag{15}$$

$$(m_h + m_p)\left(l_1\ddot{\theta} - \ddot{x}l_1\cos\theta + 2l_1\dot{l}_1\dot{\theta} + gl_1\sin\theta\right) - m_p l_1 l_2(\ddot{\varphi}\cos(\theta-\varphi) + \dot{\varphi}^2\sin(\theta-\varphi)) = 0 \tag{16}$$

$$m_p l_2\Big(-\ddot{x}\cos\varphi - 2\dot{l}_1\dot{\theta}\cos(\theta-\varphi) - l_1\ddot{\theta}\cos(\theta-\varphi) + l_1\dot{\theta}^2\sin(\theta-\varphi)\Big) + m_p\left(l_2{}^2 + \frac{1}{12}l_p{}^2\right)\ddot{\varphi} - m_p l_2\left(\ddot{l}_1\sin(\theta-\varphi) + g\sin(\theta-\varphi)\right) = 0 \tag{17}$$

$$(m_h + m_p)\Big(-\ddot{x}\sin\theta + \ddot{l}_1 - l_1\dot{\theta}^2 + g(1-\cos\theta)\Big) - m_p(\ddot{\varphi}l_2\sin(\theta-\varphi) - \dot{\varphi}l_2\sin(\theta-\varphi)) = F_l - f_l\dot{l}_1 \tag{18}$$

Eqs. (9)–(11) and (15)–(18) show that the crane system with and without payload hoisting is highly nonlinear with inextricably intertwined set of differential equations. An external force input will make the trolley to move, and consequently excite the hook and DMP to oscillate. Under the payload hoisting scenario, more complicated mathematical equations were obtained with an added independent coordinate, l_1. According to our best knowledge and the literature search, this is the first treatment of the double-pendulum crane system with DMP under hoisting with explicit equations describing the dynamics.

3. Research method

This section presents the research method utilised in this work to study the dynamic characteristics of the DPOC with DMP, and to evaluate the accuracy of the dynamic equations representing the crane system. The derived dynamic models of the DPOC without and with payload hoisting were used for simulation, whereas a laboratory DPOC was utilised in experiments. The following steps were carried out:

(a) Simulations were performed using Matlab with parameters similar to the laboratory crane. Two cases were simulated: (1) without hoisting, and (2) a simultaneous motion of trolley and payload hoisting.
(b) Experiments were carried out and comparisons with the simulation results were made to evaluate the validity and accuracy of the derived mathematical models.
(c) The dynamic behaviour of the crane was assessed in time domain. These involves the trolley motion and oscillation responses of hook and payload.
(d) The effects of carrying different DMP masses and lengths on the dynamics of the oscillation responses were studied through simulations and experimental exercises.

To assess the dynamic characteristics of the crane system with DMP and to access the accuracy of the dynamic models, the following responses and performance indexes were considered:

(a) Simulation and experimental responses of the trolley motion, hook sway angle and payload sway angle.

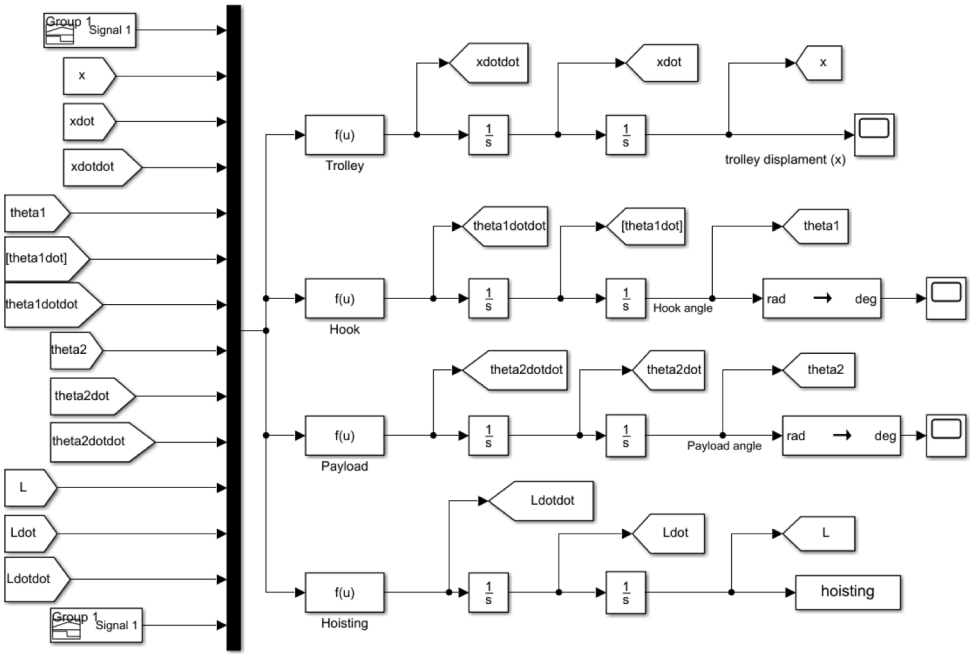

Fig. 4. Simulink block diagram.

(b) Maximum Transient Sway (MTS) and the overall sway using the Mean Absolute Error (MAE) values. Transient sway is given a special attention as the highest sway usually occurs during this phase, when the crane starts to move. MAE calculates the total oscillation throughout the observation period (0 to 10 s), and therefore a low value of MAE is desirable as it represents weak oscillation.
(c) Frequencies of the hook and payload sway responses. These are resonance frequencies that characterise the sway responses, and they are important parameters used in designing feedforward controllers based on command shaping techniques. Exact measurement and estimation of these frequencies can result in an efficient controller that guarantee significant suppression of hook and payload sways.
(d) Percentage of relative errors between simulation (theory) and experimental results for all the values described in (b) and (c).

Simulations of the non-linear dynamic equations given in Eqs. (9)–(11) and Eqs. (15)–(18) were carried out by using Matlab and Simulink. Fig. 4 illustrates the Simulink block diagram designed for the purpose of solving the non-linear equations and obtaining responses of the trolley motion, and oscillation angles of hook and DMP when excited with an external input. In this work, the *fcn* block was utilised to solve the non-linear equations. The simulations were run with the numerical integration of fifth order Runge-Kutta

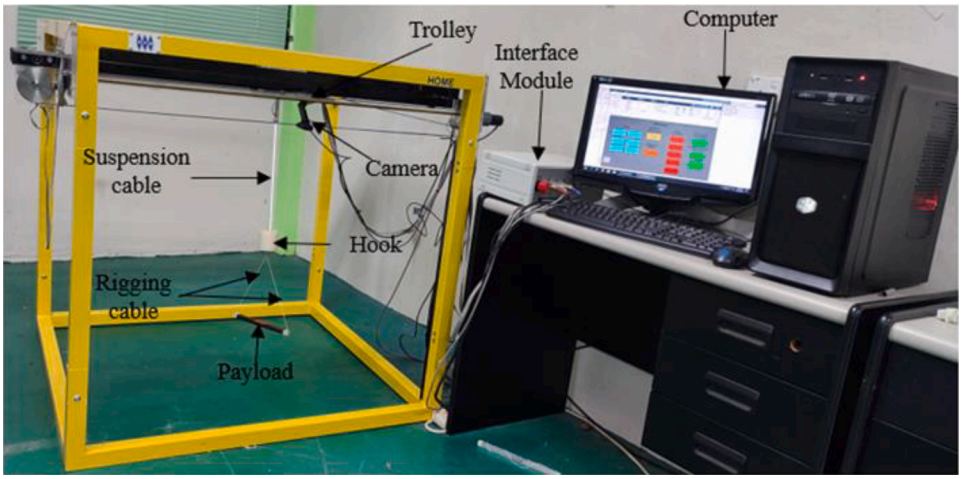

Fig. 5. The laboratory double-pendulum overhead crane with DMP.

Fig. 6. Distributed-mass payloads used in the experiments (a) Different masses with same length, (b) Same mass with different lengths.

Table 1
Double-pendulum overhead crane parameters.

Variables	Symbol	Values
Mass of trolley	m_t	1.155 kg
Mass of hook	m_h	0.1 kg
Mass of payload	m_p	0.155, 0.215, 0.275 kg
Cable length between trolley and hook	l_1	0.2 m – 0.4 m
Cable length between hook and payload	l_2	0.2 m
Length of the DMP	l_p	0.2 m, 0.305 m
Viscous damping coefficients of trolley	f_x	82 Ns/m
Viscous damping coefficients of hoisting	f_l	75 Ns/m
Gravitational constant	g	9.81/s^2

method (*ode45*) and with a sampling time of 0.001 s.

3.1. Experimental set-up

For validation of the theory and simulation results, a laboratory DPOC shown in Fig. 5 was used for experimental works. The laboratory crane has dimensions of 1 m x 1 m x 1 m, with important components labelled in Fig. 5. The hook is connected to a suspension cable and the DMP is connected to the hook through a rigging cable. Encoders are used for measurements of displacement of the trolley motion and angle of hook oscillation. For measurement of the DMP oscillation angle, a C170 camera pointing downward is attached to the trolley. The trolley and hoisting movements are driven by two separate DC motors. For communication between the crane and the computer, an RT-DAC board (interface module) is used. Furthermore, Matlab/Simulink Real-Time Toolbox is used for real-time implementation of control algorithms.

To evaluate the effects of carrying DMPs with different masses and lengths, several DMPs with different materials were carefully selected. Fig. 6 shows all the DMPs used in the experiments. In Fig. 6(a), three DMPs with the same length of 0.2 m but with different mass (0.155 kg, 0.215 kg and 0.275 kg) are shown. On the other hand, Fig. 6(b) illustrates two DMPs with different lengths (0.2 m and 0.305 m), but they have a similar mass of 0.215 kg. The parameters of the laboratory crane and DMPs are listed in Table 1. These parameters are also used in simulation of the derived dynamic equations of the motion.

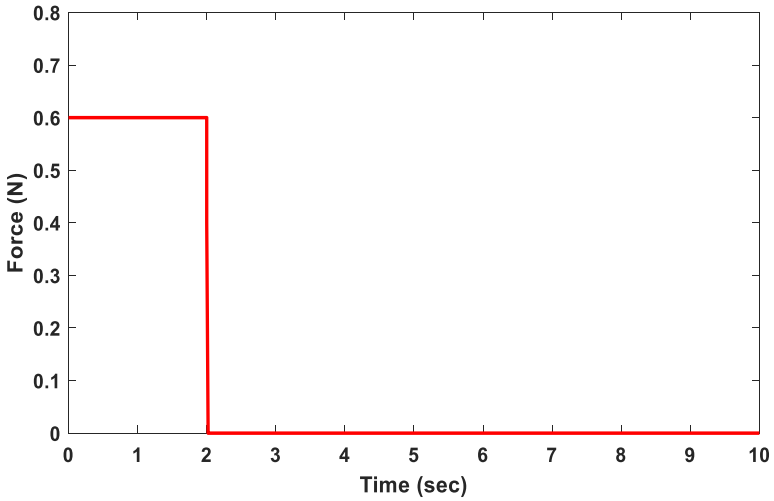

Fig. 7. Input force signal for the system.

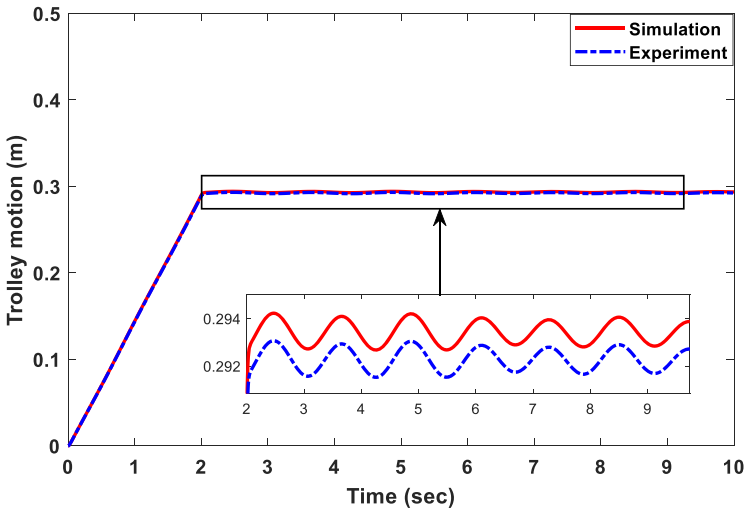

Fig. 8. Trolley position response.

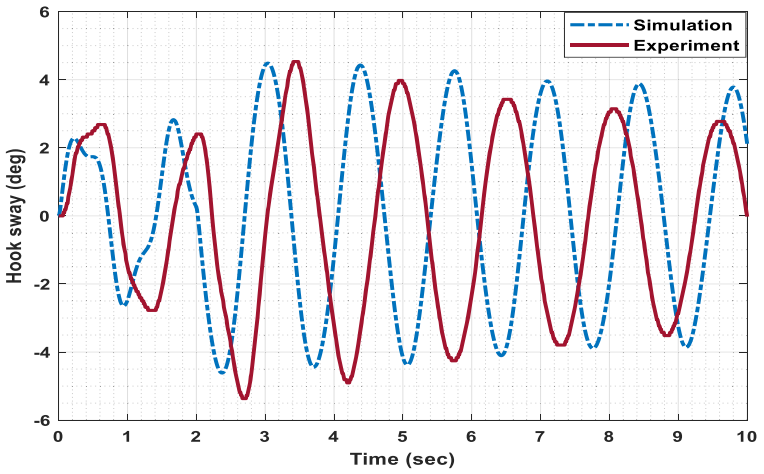

(a)

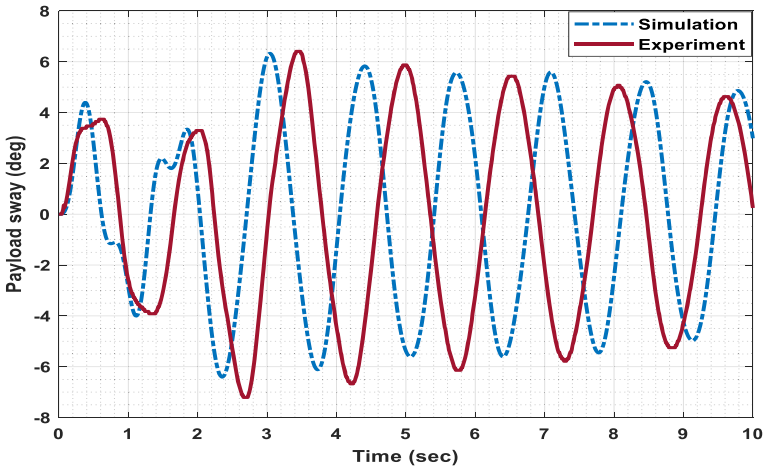

(b)

Fig. 9. Response of the DPOC with DMP without payload hoisting (a) Hook sway, (b) Payload sway.

Table 2
Performance indices measurement for the case with a fixed length.

	MTS		Frequency	
	Hook	Payload	Hook	Payload
Simulation	4.48 deg	6.32 deg	4.29 rad/s	4.06 rad/s
Experiment	4.53 deg	6.40 deg	4.25 rad/s	4.13 rad/s
Relative error (%)	1.02	1.22	0.98	1.86

4. Results and dynamic characteristic analyses

In this section, a set of simulation and experimental results are presented. These results are used to study the dynamic characteristics of the crane with DMP and the effects of changing important parameters. They are also used to validate and examine the mathematical models of the crane system. In this work, an external force of 0.6 N with a width of 2 s as shown in Fig. 7 was excited into the crane in an open loop configuration. This input force was chosen as it can move the crane to an appropriate position within the limits of the laboratory crane, and with suitable hook and DMP oscillations.

4.1. Fixed and varying cable lengths (Payload hoisting)

With a hook mass of 100 g, payload mass of 155 g and a DMP length of 0.2 m, simulation and experimental results of the trolley

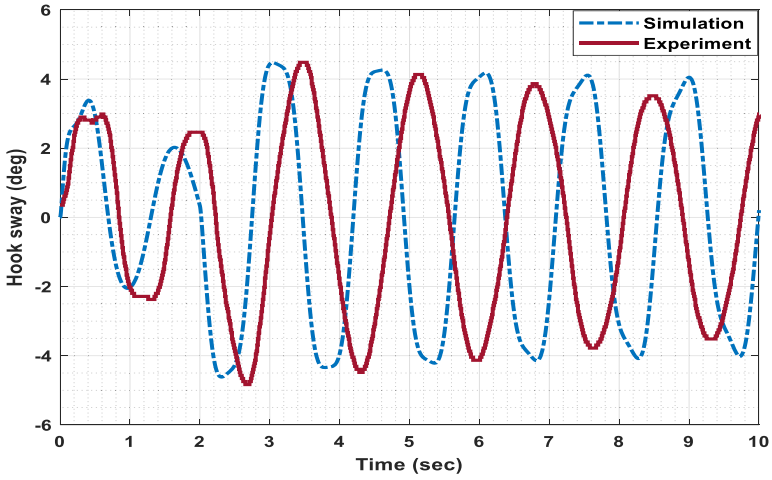

(a)

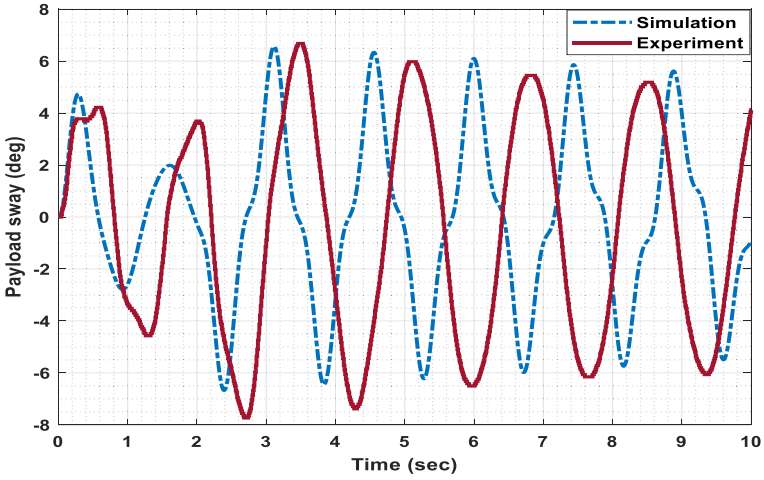

(b)

Fig. 10. Response of the DPOC with DMP with payload hoisting (a) Hook sway, (b) Payload sway.

Table 3
Performance indices measurement for the case with payload hoisting.

	MTS		Frequency	
	Hook	Payload	Hook	Payload
Simulation	4.47 deg	6.57 deg	3.88 rad/s	4.03 rad/s
Experiment	4.80 deg	6.68 deg	3.79 rad/s	3.98 rad/s
Relative error (%)	0.22	1.70	2.80	1.24

position responses to the input force are shown in Fig. 8. It is noted that both results are identical in transient and steady-state responses. Eventually, the trolley moved to a distance of about 0.29 m within 2 s. As the hook and payload oscillate during the trolley motion, and since it takes a longer time for the oscillation to settle down, the trolley response was also influenced by the oscillations. This is shown in the enlarged part of Fig. 8, in which the steady-state response of the trolley motion exhibits small and persistent oscillation. Both simulation and experiment have shown a similar trend although with slightly different values. For this particular case, a closed-loop position control might be required to achieve a precise desired trolley position.

Fig. 9(a) and (b) show the simulated and experimental results of the hook and payload oscillation responses respectively. Both results have shown that significant oscillations arise during the trolley motions. The maximum sways of payload oscillation were obtained as 4.48 deg and 4.53 deg using simulation and experiment respectively. However, it can be noted that there are slight

differences in both responses, as they were not exactly in phase. Nevertheless, both exercises provided the same pattern of responses for hook and DMP oscillations. The MTS and oscillation frequencies of the responses are tabulated in Table 2 which demonstrated closed values between the theory and experiment. The accuracy of the model was further examined based on the relative errors of MTS and frequencies as also given in Table 2. It is noted that the relative errors were less than 2%, which is small and indicates a good agreement between simulation and experimental results. Another important observation is that the hook and DMP oscillate with different frequencies, and thus it is proven that the crane with DMP is a type of multi-mode system. In this case, with experiment, the oscillation frequencies were obtained as 4.25 rad/s and 4.13 rad/s for the hook and DMP respectively.

To evaluate the effects of payload hoisting on the dynamics of DPOC, simulations and experiments were conducted with simultaneous trolley motion and payload hoisting. Due to the limitation of the laboratory crane, payload hoisting (lowering) was considered from 0.2 m to 0.4 m. Fig. 10(a) and (b) show simulation and experimental results of the hook and DMP oscillation responses respectively. Similar to the case with a fixed length, both oscillation responses were not exactly in phase. Nonetheless, the pattern of hook and DMP oscillations were identical for both simulations and experiments. For the DMP, the maximum sways were 6.57 deg and 6.68 deg, and oscillation frequencies were 4.03 rad/s and 3.98 rad/s for simulation and experiment respectively. Table 3 summarises the MTS and oscillation frequencies of the hook and DMP oscillation responses. Comparisons of those values show a close agreement between simulation and experiment with a maximum relative error of 2.80%.

The effects of DMP hoisting on the dynamics of DPOC were analysed based on the responses in Figs. 9 and 10. It was revealed that the oscillation behaviour in terms of their magnitudes, shapes and frequencies are affected by varying cable length during simultaneous motion of trolley and payload hoisting operation. Similar effects on the DPOC dynamics can be observed in simulation and experiment. With the hoisting operation, the simulated MTS value has reduced by 0.2% for hook, and has increased by 3.9% for DMP. Experiment shows a similar trend with 1.3% reduction for the hook and 4.2% increment for the payload. On the other hand, the

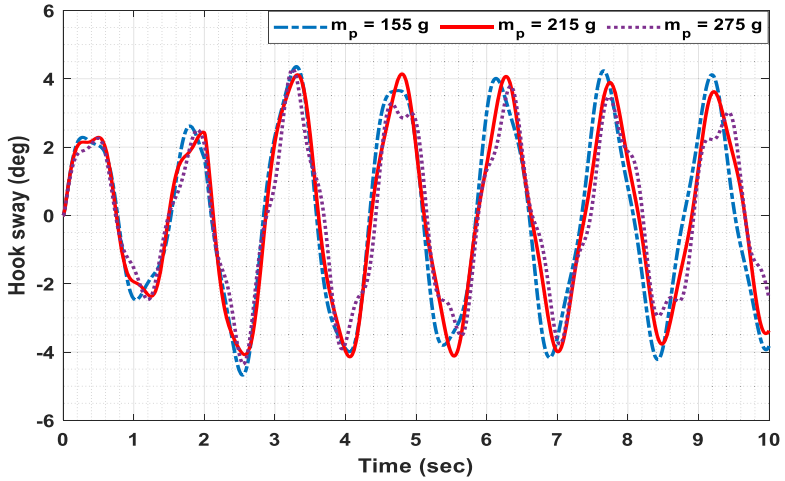

(a)

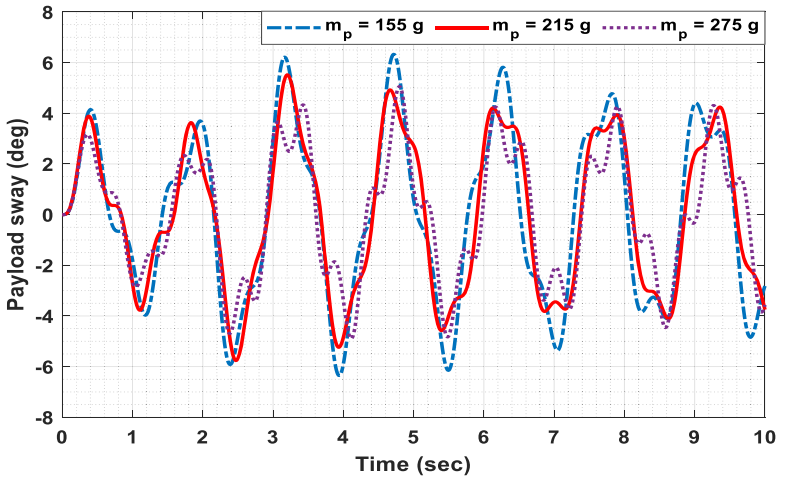

(b)

Fig. 11. Simulated response of the DPOC with DMP under mass variations (a) Hook sway, (b) Payload sway.

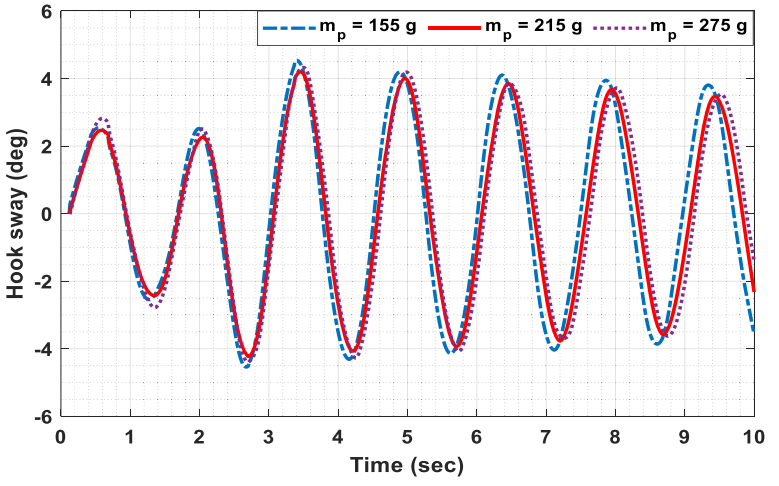

(a)

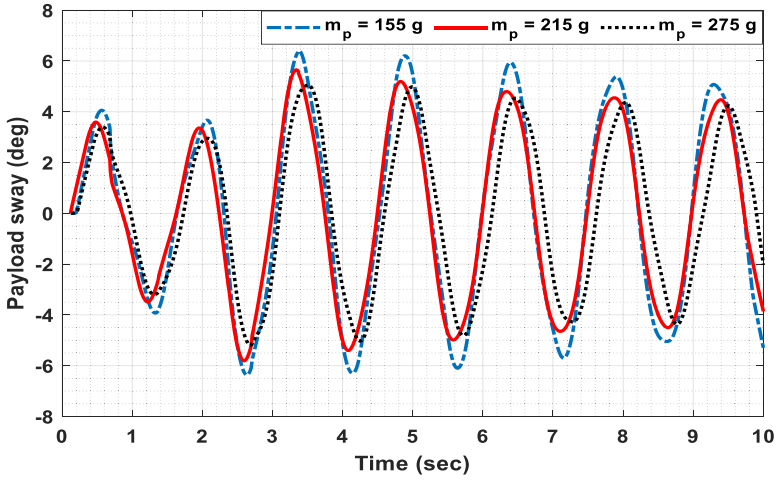

(b)

Fig. 12. Experimental response of the DPOC with DMP under mass variations (a) Hook sway, (b) Payload sway.

Table 4
Performance indices and frequencies under payload mass variations.

(g)	Simulation						Experiment					
	Hook			Payload			Hook			Payload		
	MTS (deg)	MAE	ω_h (rad/s)	MTS (deg)	MAE	ω_p (rad/s)	MTS (deg)	MAE	ω_h (rad/s)	MTS (deg)	MAE	ω_p (rad/s)
155	4.49	2.35	4.28	6.33	2.87	4.06	4.53	2.38	4.25	6.41	3.41	4.13
215	4.14	2.21	4.21	5.52	2.62	4.33	4.20	2.24	4.19	5.65	2.94	4.19
275	4.28	1.96	4.49	5.06	2.17	4.59	4.33	2.03	4.30	5.06	2.73	4.41

average oscillation frequencies of hook and payload have reduced by 11.7% and 4.4% respectively in simulation, whereas the frequencies have reduced by 10.8% and 3.6% in experiment. These concur with the theory as increasing the cable length during payload hoisting (lowering) results in a lower oscillation frequency.

The slight differences between simulation and experimental results, in which the responses were not in phase, together with the percentage relative errors might be due to several assumptions used in the modelling process and several factors which were ignored. These include air friction and wind disturbance which were not taken into account in the model derivation. Nevertheless, for both cases with and without payload hoisting, simulations and experiments provided the same patterns in the system's dynamic behaviour with small relative errors in MTS and oscillation frequencies. The good compliance between the model and the plant response indicates the

Table 5
Percentage of relative errors between simulation and experimental results under mass variations.

Payload mass (g)	Hook (%)			Payload (%)		
	MTS	MAE	Frequency	MTS	MAE	Frequency
155	0.8	1.2	0.7	1.2	15.8	1.7
215	1.4	1.3	0.5	2.3	10.4	3.3
275	1.1	3.4	4.2	0	20.5	3.9

usefulness of the model for feedforward and feedback controller designs.

4.2. The effects of payload mass variations

This section evaluates the effects of payload mass variations on the dynamic behaviour of the DPOC with DMP. It is essential to study these effects as cranes are used to carry different payload masses during their operations. In these investigations, payload masses of 155 g, 215 g and 275 g as shown in Fig. 6(a) were used, while other parameters are kept constants: cable length 0.3 m, hook mass 100 g and payload length 0.2 m.

Figs. 11 and 12 show simulation and experimental sway responses respectively. It can be observed that by carrying different payload masses, the hook and payload responses were considerably affected, especially in terms of its magnitude, shape and frequency.

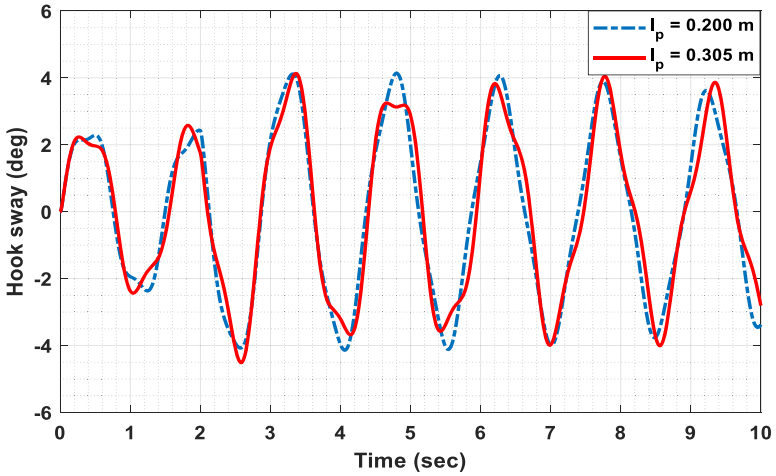

(a)

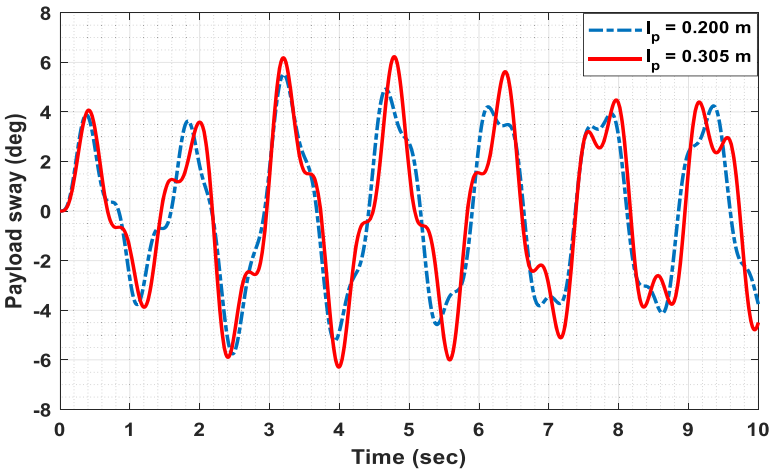

(b)

Fig. 13. Simulated response of the DPOC with DMP under different payload lengths (a) Hook sway, (b) Payload sway.

Table 4 summarises the MTS, MAE and sway frequencies values of the oscillations for simulation and experiment. As payload mass increases, it can be observed in both cases, that MTS for payload and MAE for the hook and payload decrease. This indicates that a larger mass yields a lower crane oscillation. For the payload sway, simulated MTS and MAE values have reduced by 20% and 24.4% respectively when the mass was changed from 155 g to 275 g whereas, the MTS and MAE values have reduced by 21% and 20% in experiments. However, the MTS values for the hook sway show a mixed pattern with increasing payload masses. Additionally, in both simulation and experiment, the sway frequency for payload increases with increasing payload. The increments were calculated as 12% and 3% for the simulation and experiment respectively. Similar to the case with MTS, the hook frequency shows a mixed pattern with the three payload masses.

The accuracy of the dynamic model with various payload masses was further examined by conducting detailed comparisons with the experimental results. Table 5 summarises the percentage of relative errors for MTS, MAE and sway frequencies for the hook and

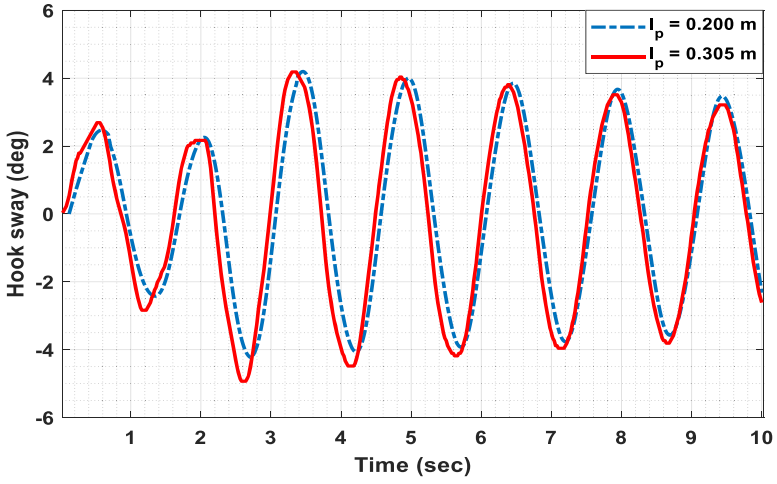

(a)

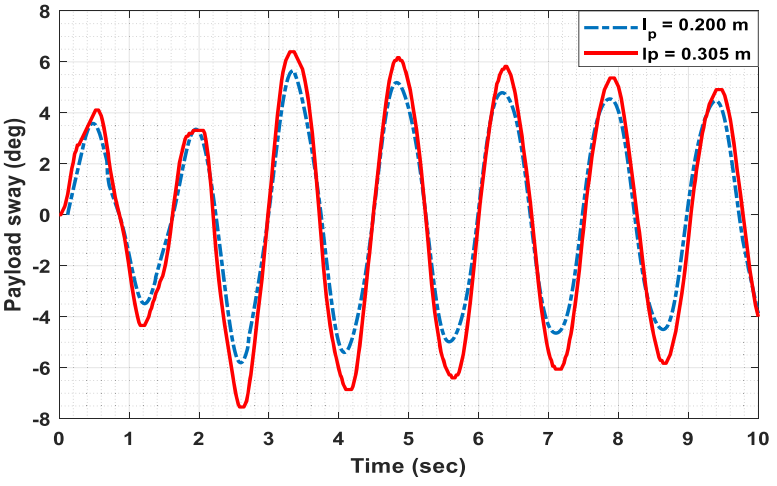

(b)

Fig. 14. Experimental response of the DPOC with DMP under different payload lengths (a) Hook sway, (b) Payload sway.

Table 6
Performance indices and frequencies under payload length variations.

(cm)	Simulation						Experiment					
	Hook			Payload			Hook			Payload		
	MTS (deg)	MAE	ω_h (rad/s)	MTS (deg)	MAE	ω_p (rad/s)	MTS (deg)	MAE	ω_h (rad/s)	MTS (deg)	MAE	ω_p (rad/s)
20.0	4.14	2.21	4.13	5.52	2.62	4.19	4.20	2.24	4.09	5.65	2.94	4.13
30.5	4.13	2.16	4.03	6.23	2.69	4.03	4.18	2.19	4.08	6.39	3.61	4.08

Table 7
Percentage of relative errors between simulation and experimental results under different payload lengths.

Payload length (m)	Hook (%)			Payload (%)		
	MTS	MAE	Frequency	MTS	MAE	Frequency
0.200	1.4	1.3	1.0	2.3	10.8	1.5
0.305	1.2	1.4	1.2	1.7	25.5	1.2

payload responses. With the exception of payload's MAE, all relative errors were below 5%, indicating a close agreement between simulation and experiment. Higher percentage errors with the MAE of the payload oscillation were due to the simulation responses at the peak magnitudes, which were not as smooth as the experimental results. Nevertheless, the magnitude and the frequency of the emerged oscillations are similar in both works, which are useful for further analyses and for controller design.

4.3. The effects of payload length variations

In some practical cases, the DPOC is required to carry DMPs with different lengths. This section investigates the effects of payload length variations on the dynamics of the hook and payload oscillations. Two different payload lengths of 0.20 m and 0.305 m as shown in Fig. 6(b) were considered, with the other parameters remain constants, i.e., payload mass of 215 g and cable length of 0.3 m.

With the same input force as in Section 4.1, simulation and experimental results of the sway responses with different payload lengths are illustrated in Figs. 13 and 14 respectively, and Table 6 summarizes the MTS, MAE and oscillation frequency values. With these two payload lengths, it can be observed that the hook oscillation was not much affected. In this case, the MTS values were quite similar, whereas the MAE values have reduced only by 2% in both exercises. In contrast, the payload oscillations were considerably affected. By increasing the payload length from 0.2 m to 0.305 m, the MTS values have increased by 12.9% and 12.2%, and the MAE values have increased by 2.7% and 22.8% for simulation and experiment respectively. It is noted that with increasing DMP length, there were slight increments in the oscillation frequencies. The frequencies of the hook sway have increased by 2.4% and 0.2% with simulation and experiment respectively, whereas the payload's frequencies have increased by 3.8% and 1.2%.

Similarly, to examine the accuracy of the dynamic models, the percentages of relative errors between simulation and experiment were calculated. Table 7 shows the percentage errors with two payload lengths. Apart from payload's MAE, all the relative errors were below 3%, which again show a close agreement between simulation and experiment. Similar to the result in the previous section, the simulated payload sway was not as smooth as the experimental result, which contributes to the high percentage of the relative errors for MAE.

5. Conclusion

This paper presents a comprehensive analysis of the dynamic characteristics of a double-pendulum overhead crane (DPOC) when carrying a distributed-mass payload (DMP). It encompasses the development and simulation of nonlinear dynamic models for the crane, both with and without DMP hoisting. The study also delves into the impact of varying cable lengths, distinct payload masses, and different payload lengths on the dynamics of hook and payload oscillations. To validate the derived models and to assess their accuracy, experiments were conducted using a laboratory crane. The results from both simulation and experimentation highlight the substantial influence of these parameters on payload oscillation. The devised model is validated experimentally, and the experimental results are in very good compliance with the theory. Future work will investigate the effects of larger DMP masses and longer DMP lengths to further validate the accuracy of the models. In addition, dynamic characterisations of cranes with DMP oscillation and twisting will also be considered.

Declaration of competing interest

None.

Data availability

No data was used for the research described in the article.

References

[1] W. Singhose, Command shaping for flexible systems: a review of the first 50 years, Int. J. Precis. Eng. Manuf. 10 (2009) 153–168.
[2] L. Ramli, Z. Mohamed, A.M. Abdullahi, H.I. Jaafar, I.M. Lazim, Control strategies for crane systems: a comprehensive review, Mech. Syst. Signal Process. 95 (2017) 1–23.
[3] K.S. Hong, U.H. Shah, Introduction, in: K.S. Hong, U.H. Shah (Eds.), Dyn. Control Ind. Cranes, Springer, Singapore, 2019, pp. 1–9.
[4] T.Y. Jian, Z. Mohamed, Modelling and sway control of a double-pendulum overhead crane system, Appl. Model. Simul. 1 (2017) 15–21.
[5] X. Zhao, J. Huang, Distributed-mass payload dynamics and control of dual cranes undergoing planar motions, Mech. Syst. Signal Process. 126 (2019) 636–648.
[6] M.R. Mojallizadeh, B. Brogliato, C. Prieur, Modeling and control of overhead cranes: a tutorial overview and perspectives, Annu. Rev. Control. (2023) 100877.

[7] J. Huang, Z. Liang, Q. Zang, Dynamics and swing control of double-pendulum bridge cranes with distributed-mass beams, Mech. Syst. Signal Process. 54–55 (2015) 357–366.
[8] R. Tang, J. Huang, Control of bridge cranes with distributed-mass payloads under windy conditions, Mech. Syst. Signal Process. 72–73 (2016) 409–419.
[9] J. Peng, J. Huang, W. Singhose, Payload twisting dynamics and oscillation suppression of tower cranes during slewing motions, Nonlinear Dyn. 98 (2019) 1041–1048.
[10] Z. Sun, H. Ouyang, Adaptive fuzzy tracking control for vibration suppression of tower crane with distributed payload mass, Autom. Constr. 142 (2022) 104521.
[11] Q. Wu, X. Wang, L. Hua, M. Xia, Dynamic analysis and time optimal anti-swing control of double pendulum bridge crane with distributed mass beams, Mech. Syst. Signal Process. 144 (2020) 106968.
[12] X. Miao, L. Yang, H. Ouyang, Artificial-neural-network-based optimal smoother design for oscillation suppression control of underactuated overhead cranes with distributed mass beams, Mech. Syst. Signal Process. 200 (2023) 110497.
[13] J. Ye, J. Huang, Control of beam-pendulum dynamics in a tower crane with a slender jib transporting a distributed mass load, IEEE Trans. Ind. Electron. 70 (2023) 888–897.
[14] T. Wang, N. Tan, X. Zhang, G. Li, S. Su, J. Zhou, J. Qiu, Z. Wu, Y. Zhai, R. Donida Labati, V. Piuri, F. Scotti, A time-varying sliding mode control method for distributed-mass double pendulum bridge crane with variable parameters, IEEE Access 9 (2021) 75981–75992.
[15] Q. Wu, N. Sun, X. Wang, Equivalent rope length-based trajectory planning for double pendulum bridge cranes with distributed mass payloads, Actuators 11 (2022) 25.
[16] Q. Wu, X. Wang, L. Hua, M. Xia, Improved time optimal anti-swing control system based on low-pass filter for double pendulum crane system with distributed mass beam, Mech. Syst. Signal Process. 151 (2021) 107444.
[17] L. Yang, H. Ouyang, Precision-positioning adaptive controller for swing elimination in three-dimensional overhead cranes with distributed mass beams, ISA Trans. 127 (2022) 449–460.
[18] Q. Wu, N. Sun, T. Yang, Y. Fang, Deep reinforcement learning-based control for asynchronous motor-actuated triple pendulum crane systems with distributed mass payloads, IEEE Trans. Ind. Electron. 71 (2024) 1853–1862.
[19] H.M. Cuong, L.A. Tuan, Robust control of rubber–tyred gantry cranes with structural elasticity, Appl. Math. Model. 117 (2023) 741–761.
[20] E.I. Kaptsov, S.V. Meleshko, Analysis of the one-dimensional Euler–Lagrange equation of continuum mechanics with a Lagrangian of a special form, Appl. Math. Model. 77 (2020) 1497–1511.
[21] H.I. Jaafar, Z. Mohamed, M.A. Shamsudin, N.A. Mohd Subha, L. Ramli, A.M. Abdullahi, Model reference command shaping for vibration control of multimode flexible systems with application to a double-pendulum overhead crane, Mech. Syst. Signal Process. 115 (2019) 677–695.